Propagation of Tracer Signals in Boundary Currents

DARRYN W. WAUGH

Department of Earth and Planetary Sciences, The Johns Hopkins University, Baltimore, Maryland

TIMOTHY M. HALL

NASA Goddard Institute for Space Studies, New York, New York

(Manuscript received 31 July 2004, in final form 19 December 2004)

ABSTRACT

The propagation of a range of tracer signals in a simple model of the deep western boundary current is examined. Analytical expressions are derived in certain limits for the transit-time distributions and the propagation times (tracer ages) of tracers with exponentially growing or periodic concentration histories at the boundary current's origin. If mixing between the boundary current and the surrounding ocean is either very slow or very rapid, then all tracer signals propagate at the same rate. In contrast, for intermediate mixing rates tracer ages generally depend on the history of the tracer variations at the origin and range from the advective time along the current to the much larger mean age. Close agreement of the model with chlorofluorocarbon (CFC) and tritium observations in the North Atlantic deep western boundary current (DWBC) is obtained when the model is in the intermediate mixing regime, with current speed around 5 cm s^{-1} and mixing time scale around 1 yr. In this regime anomalies in temperature and salinity of decadal or shorter period will propagate downstream at roughly the current speed, which is much faster than the spreading rate inferred from CFC or tritium–helium ages (approximately 5 cm s^{-1} as compared with 2 cm s^{-1}). This rapid propagation of anomalies is consistent with observations in the subpolar DWBC, but is at odds with inferences from measurements in the tropical DWBC. This suggests that observed tropical temperature and salinity anomalies are not simply propagated signals from the north. The sensitivity of the tracer spreading rates to tracer and mixing time scales in the model suggests that tight constraints on the flow and transport in real DWBCs may be obtained from simultaneous measurements of several different tracers—in particular, hydrographic anomalies and steadily increasing transient tracers.

1. Introduction

Deep western boundary currents (DWBCs) play an important role in ocean circulations and the climate system. In these currents waters formed in polar and subpolar regions flow into other regions, and even the other hemisphere, transporting freshwater and anthropogenic carbon. Quantifying this transport is thus important for understanding the ocean's role in redistributing heat, propagating climate anomalies formed in polar regions, and sequestering anthropogenic carbon.

Estimates of the current speeds and effective transport rates in these boundary currents have been obtained from a variety of measurements, including direct measurements of the velocities, measurements of temperature and salinity, measurements of transient tracers such as chlorofluorocarbons (CFCs) and tritium, and the movement of subsurface floats. Generally the transport rates inferred from these data differ. For example, mean velocities in the North Atlantic Ocean DWBC from current meters are 5–10 cm s^{-1} (e.g., Watts 1991; Pickart and Smethie 1998), whereas the spreading rates inferred from hydrographic anomalies are 2–2.5 cm s^{-1} (e.g., Molinari et al. 1998; Freudenthal and Andrie 2002) and those inferred from transient tracer ages are 1–2 cm s^{-1} (e.g., Doney and Jenkins 1994; Smethie et al. 2000; Fine et al. 2003).

It is now recognized that the differences among these estimates are primarily due to mixing and recirculation (e.g., Pickart et al. 1989; Doney and Jenkins 1994). A wide range of pathways and transit times are available from the surface to points along the DWBC, and the net effect is to reduce the propagation rate of tracer

Corresponding author address: Darryn W. Waugh, Department of Earth and Planetary Sciences, The Johns Hopkins University, 3400 N. Charles, Baltimore, MD 21218.
E-mail: waugh@jhu.edu

© 2005 American Meteorological Society

Unauthenticated | Downloaded 05/20/24 05:05 AM UTC

signals below that of pure advection along the DWBC core. However, while past studies have elucidated important aspects of the relationship between tracer propagation and flow, the variety of responses over the full set of available tracers has not yet been examined. We would like to know how sensitive the propagation rates of these tracers are to the nature and details of their histories at the DWBC origin and how the propagation rates depend on the balance of bulk advection and mixing. Addressing these questions will, among other things, provide insight into how best to use tracer measurements to infer aspects of the flow and transport in DWBCs.

One could address these questions by performing experiments in a numerical model that produced a DWBC by solving dynamical equations. However, it is difficult in such models to vary individually quantities such as the size and speed of boundary currents and the rate of mixing between regions. In this study we use a simple kinematical model of the DWBC in which the transport rates of interest are parameters that can be directly varied. The model is very similar to models employed in several past DWBC studies (e.g., Pickart et al., 1989; Doney and Jenkins, 1994; Rhein 1994; Haine et al. 1998). The DWBC is represented as a one-dimensional advective–diffusive region that exchanges water and tracer with a much larger, more slowly moving ocean interior region. In certain limits we obtain analytical expressions for the transit-time distribution (TTD) and for the evolution of idealized tracers with exponentially or periodically varying concentration histories. Using these solutions we examine and interpret the propagation of realistic tracers, including temperature and salinity anomalies.

In the next section the model is presented and compared with other similar models used in past studies: The transit-time distribution in this model is presented and discussed in section 3. In section 4 idealized tracers with exponential growth or periodic variations are examined. The propagation of realistic tracers (e.g., CFCs and tritium) is examined in section 5, and model results are compared with observations. In section 6 the robustness of the conclusions drawn from this analysis is assessed by relaxing the limits that allow analytical solution and by comparing with a commonly used one-dimensional advection–diffusion model. Concluding remarks are in the final section.

2. Model

For our analysis we wish to use a model that is as simple as possible but still includes the key transport processes in DWBCs. Several previous studies have used one-dimensional flow with constant velocity and diffusion (1D advection–diffusion) when examining transient tracers and transport time scales (e.g., Sonnerup 2001; Wunsch 2002; Klatt et al. 2002; Waugh et al. 2003; Steinfeldt and Rhein 2004). However, the dominant mixing in the DWBC occurs laterally between the boundary current and interior region, not in the direction of the flow. We therefore use an alternative model consisting of two coupled regions, a narrow advective–diffusive boundary current with rapid, uniform flow and a larger, more slowly moving interior region. Mixing of tracer between the two regions is parameterized as simple relaxation with time constant t_{mix}.

The partitioning of the cross-sectional DWBC structure into two laterally uniform regions is clearly unrealistic. Observations show a gradual decline in transit tracer concentration from a peak in the DWBC core to much lower ambient levels at distance. Our primary purpose, however, is to examine the tracer structure and propagation along the current, not across. Thus, it is reasonable to average over the lateral structure and use a single exchange time scale, t_{mix}, to summarize mixing between the averaged boundary current state and averaged interior state. Pickart et al. (1989) motivate the structure of this type of model in more detail and relate t_{mix} to lateral diffusivities.

In its most general form the tracer continuity equations for the DWBC model are

$$\frac{\partial \chi_b}{\partial t} + u_b \frac{\partial \chi_b}{\partial x} + \kappa_b \frac{\partial^2 \chi_b}{\partial x^2} + \frac{1}{t_{\text{mix}}}(\chi_b - \chi_i) = S_b \quad \text{and} \tag{1}$$

$$\frac{\partial \chi_i}{\partial t} + u_i \frac{\partial \chi_i}{\partial x} + \kappa_i \frac{\partial^2 \chi_i}{\partial x^2} - \frac{\alpha}{t_{\text{mix}}}(\chi_b - \chi_i) = S_i, \tag{2}$$

where x is the distance along the current; the b and i subscripts correspond to quantities in the boundary current and interior regions, respectively; $\chi(x, t)$ are the tracer concentrations; u is the flow in the x direction; κ is the along-flow diffusivity; $S(x, t)$ is the tracer source or sink; and $\alpha = \delta_b/\delta_i$ is the ratio of the width of the boundary current to that of the interior region. The model used is illustrated in Fig. 1 (see Table 1 for a glossary of symbols). Boundary conditions on χ_b are applied at $x = 0$.

In much of our analysis we make further simplifications. First, scaling arguments (Pickart et al. 1989) show readily that along-flow diffusion is negligible relative to lateral mixing. For example, a tracer whose concentration varies on a scale of d along the DWBC would have to experience a diffusivity $\kappa \sim d^2/t_{\text{mix}}$ for diffusion to compete with lateral mixing. Typical time scales for lateral exchange are 1–2 yr and typical length scales of

Unauthenticated | Downloaded 05/20/24 05:05 AM UTC

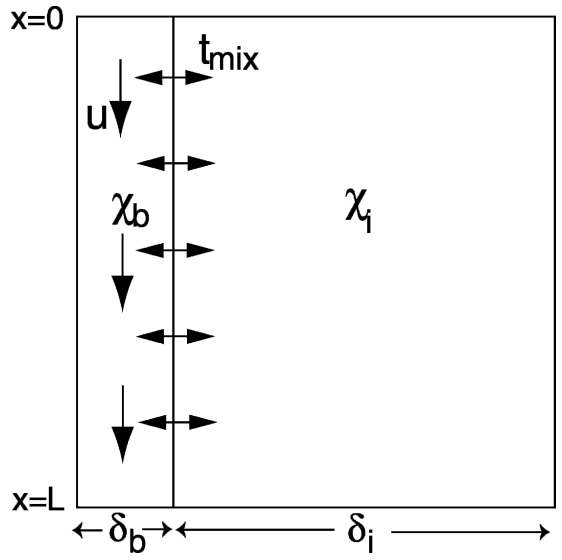

FIG. 1. Schematic of boundary current model. The model consists of two regions, a boundary current with width δ_b and uniform flow u and larger interior region with width δ_i ($>\delta_b$) and no flow. Mixing between the regions is parameterized as relaxation with time scale t_{mix}; $\chi_b(x, t)$ and $\chi_i(x, t)$ are the tracer concentrations in the boundary current and interior region.

TABLE 1. Explanation of symbols.

Symbol	Definition	Type
u	Current speed	Model parameter
α	Ratio of current to interior width	Model parameter
t_{mix}	Current interior mixing time	Model parameter
$t_{\text{adv}} = x/u$	Advective time	Constrained parameter
$P = t_{\text{mix}}/t_{\text{adv}}$	Peclet number	Constrained parameter
Γ	Mean transit time	Computed diagnostic
σ	Standard deviation of TTD	Computed diagnostic
T_{exp}	Time scales of exponentially increasing tracer	Tracer parameter
T_ω	Period of periodic tracer	Tracer parameter
τ_{exp}	Age of exponentially increasing tracer	Computed diagnostic
τ_ω	Phase lag of periodic tracer	Computed diagnostic
A_ω	Amplitude of periodic tracer	Computed diagnostic

tracer structure are order 10^3 km, yielding a requirement of $\kappa \sim 10^7$ m^2 s^{-1}. This is three orders of magnitude larger than independent estimates of isopycnal eddy diffusion (e.g., Ledwell et al. 1998), and thus we consider $\kappa_b = 0$. Second, we neglect all motion in the interior region ($u_i = 0$ and $\kappa_i = 0$). This seemingly severe restriction turns out to have little impact on transient tracers in the boundary current region. The principle effect of the interior is to delay the propagation of water mass fractions along the boundary current. Water and tracer enter the interior and must return to the boundary current before they can continue their propagation. Whether or not they advect or diffuse a small amount while in the interior makes little difference. Note that Pickart et al. (1989) and Doney and Jenkins (1994) also neglected these processes in their idealized models of DWBCs. In section 6 we examine in a numerical version of the model the impact on tracers of allowing the interior region to advect the small amount necessary to balance the net mass flow.

With these simplifications the tracer continuity equations reduce to

$$\frac{\partial \chi_b}{\partial t} + u\frac{\partial \chi_b}{\partial x} + \frac{1}{t_{\text{mix}}}(\chi_b - \chi_i) = S \quad \text{and} \tag{3}$$

$$\frac{\partial \chi_i}{\partial t} - \frac{\alpha}{t_{\text{mix}}}(\chi_b - \chi_i) = S, \tag{4}$$

and analytical expressions can be derived from transit time distributions and a large range of tracers (see following sections).

As mentioned above, several other studies have considered "pipe" models similar to the above reduced DWBC model. Doney and Jenkins (1994) considered a model the same as that above except that the area of the interior region increased downstream. (They expressed the exchange between regions in terms of a coefficient $\kappa = A_b/t_{\text{mix}}$, where $A_b = \delta_b L$ is the area of the boundary current.) Doney and Jenkins examined the propagation of tritium and excess helium (^{3}He) in this model, but did not present results for other tracers. They presented numerical solutions for a flow configuration with $A_b = 0.8 \times 10^8$ m^2 and interior area A_i increasing from 0.6×10^8 to 2.2×10^8 m^2, and showed that the model could reproduce the main features of the observed tritium and excess helium in the North Atlantic DWBC when $u = 5$ cm s^{-1} and κ is between 1.2 and 2 m^2 s^{-1}. In terms of the parameters in Eqs. (3) and (4), this corresponds to α between 0.03 and 0.13 and t_{mix} between 1.3 and 2.1 yr

Pickart et al. (1989), Rhein (1994), and Haine et al. (1998) also considered pipe models of DWBCs. In the models of Pickart et al. there are three regions: an inner advective core, an adjacent shoulder region that exchanges with the core and accumulates tracers, and an infinite surrounding region that is tracer free. Pickart et al. considered two versions, one where the core and shoulder regions have equal cross-sectional area and

Unauthenticated | Downloaded 05/20/24 05:05 AM UTC

there is no motion in the shoulder region and another where there is flow in a shoulder region with larger area than the core. Comparisons of CFC measurements in the DWBC near the Grand Banks with both models yielded core speeds of 5–10 cm s^{-1} and lateral diffusivities (for mixing between the core and shoulder region) $O(10^6)$ cm^2 s^{-1}.

The model defined by Eqs. (3) and (4) is also similar to the "leaky pipe" models used to model transport in the stratosphere (e.g., Neu and Plumb 1999; Hall 2000; Hall and Waugh 2000). The stratospheric leaky pipe models couple a tropical region to two midlatitude regions, have density decreasing with height (distance along the pipe) and have reverse flow in the midlatitude regions (constrained by mass continuity). Because of the along-flow density variations the details of the solutions to these models differ from the solutions presented below, but many qualitative features carry over.

3. Transit-time distributions

We first consider the time scales for transport in the DWBC model. [Unless otherwise stated we consider the reduced DWBC model defined by Eqs. (3) and (4).] Several recent studies have highlighted the fact that there is no single time for transport from one location to another in the oceans, but rather a distribution of transit times (e.g., Beining and Roether 1996; Deleersnijder et al. 2001; Khatiwala et al. 2001; Haine and Hall 2002). These transit-time distributions correspond to boundary Green's functions that propagate a boundary condition on tracer concentration from a specified region into the interior (Hall and Plumb 1994; Holzer and Hall 2000; Haine and Hall 2002). That is,

$$\chi(x, t) = \int_0^\infty \chi(0, t - \xi)\mathcal{G}(x, \xi)e^{-\lambda\xi}\, d\xi, \qquad (5)$$

where $\chi(0, t)$ is the known tracer concentration history at $x = 0$, and $\mathcal{G}(x, \xi)$ is the propagator, or TTD, with the interpretation that $d\xi\mathcal{G}(x, \xi)$ is the mass fraction of the water at x that had last contact with $x = 0$ an elapsed time ξ to $\xi + d\xi$. The factor $e^{-\lambda\xi}$ represents the radioactive decay of the tracer with decay rate λ; that is, $S_{b,i} = -\lambda\chi_{b,i}$ in Eq. (1). TTDs provide a fundamental description of the transport in a flow and are independent of any particular tracer.

The TTD in the boundary current of our model is (see the appendix)

$$\mathcal{G}(x, t) = \hat{G}_1\delta(t - t_{\text{adv}}) + \hat{G}_2\Theta(t - t_{\text{adv}}), \qquad (6)$$

where

$$\hat{G}_1 = e^{-t_{\text{adv}}/t_{\text{mix}}} \quad \text{and}$$

$$\hat{G}_2 = \frac{\alpha}{\zeta t_{\text{mix}}}\, e^{-(1+\zeta^2)t_{\text{adv}}/t_{\text{mix}}} I_1(2\zeta t_{\text{adv}}/t_{\text{mix}}),$$

$t_{\text{adv}} = x/u$ is the bulk advective time to reach position x, $\zeta^2 = (\alpha u/x)(t - x/u)$, I_1 is the modified Bessel function of first order, δ is Dirac delta function, and Θ is the Heaviside function. The combination $t_{\text{mix}}/t_{\text{adv}}$ can be interpreted as a Peclet number summarizing the relative roles of mixing and advection to point x. In Eq. (6), and equations below, only the solutions within the boundary current are presented, and we drop the subscript b. Full solutions for the boundary current and interior are given in the appendix.

Figure 2 shows TTDs for $u = 5$ cm s^{-1} (1575 km yr^{-1}), $x = 1575$ km ($t_{\text{adv}} = 1$ yr), fractional area of the boundary current $\alpha = 0.1$, and several different mixing times t_{mix}. [As it is not possible to plot a literal delta function, the term $\hat{G}_1\delta(t - x/u)$ is shown in these plots as a box of width ϵ and height $\hat{G}_1/\epsilon$, with $\epsilon = 0.05$ yr.] If only advection is present the TTD in the boundary current is a delta function at the advective time t_{adv}; that is, $\hat{G}_1 \to 1$ and $\hat{G}_2 \to 0$ as $t_{\text{mix}} \to \infty$. When mixing between the boundary current and interior is added the advective spike is still present, but its magnitude is weaker ($\hat{G}_1 < 1$), and there is a "tail" due to water of various ages mixing back into the boundary current (e.g., Figs. 2a,b). As the mixing increases (smaller t_{mix}) the relative contribution due to direct advection in the current decreases ($\hat{G}_1 \to 0$) and the TTD is dominated by older waters that have mixed with the interior (e.g., Figs. 2c,d). The TTDs for the interior region are similar but have no advective spike and are shifted to slightly older times (not shown). For different values of α the detailed form of the TTDs differ, but the general shape and variations with t_{mix} are as shown in Fig. 2. In the presence of along-flow diffusion of realistic magnitude the unphysical delta functions in the TTDs are replaced by narrow, but finite, peaks of approximately Gaussian shape. As discussed previously, the effect on tracers is negligible.

The variation of the TTDs in the boundary current with distance downstream is shown in Fig. 3, for $t_{\text{mix}} = 1$ yr and $\alpha = 0.1$ (cf. with Fig. 2b). At all locations the TTDs have an early narrow peak, due to advective transport, and a weak broad tail, due to water that has recirculated through the interior region. The advective peak occurs at later times for larger distances from the source, as it takes longer for the advective flow to reach

Unauthenticated | Downloaded 05/20/24 05:05 AM UTC

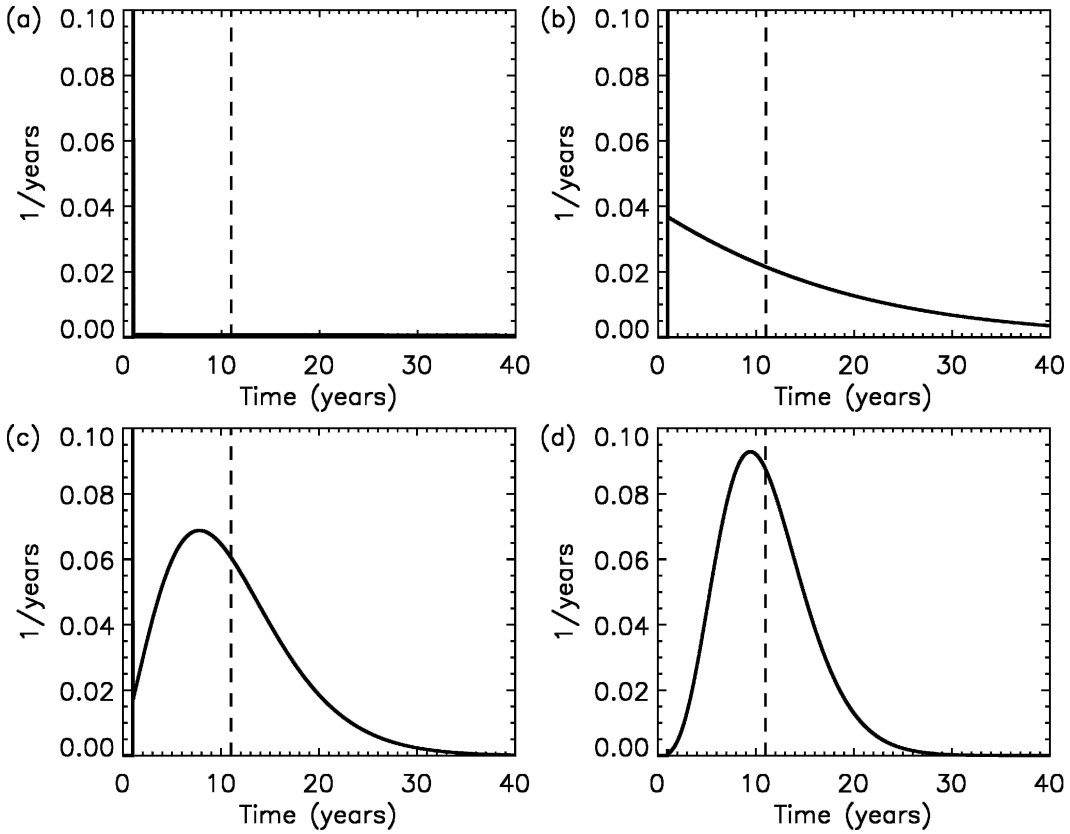

FIG. 2. TTDs for DWBC model with fractional boundary current width $\alpha = 0.1$, $u = 5$ cm s^{-1} (1575 km yr^{-1}), $x = 1575$ km (advective time $t_{adv} = 1$ yr), and mixing time t_{mix} = (a) 10, (b) 1, (c) 0.2, and (d) 0.1 yr. The vertical dashed lines show the mean transit time Γ.

the location. In the two locations nearest the source the TTDs decrease monotonically for time older than the peak time, but for locations farther downstream there is a second, much older, peak in the TTDs. Also, the relative contribution of the advective spike decreases with distance from the source. At 12 600 km (approximate distance along the North Atlantic DWBC from Denmark Strait to the tropical Atlantic) the advective peak at 8 yr is very small and the TTD is dominated by the tail, which has a peak around 70 yr.

The mean transit time (sometimes called "mean age" or "ideal age") of the boundary current TTD is (see the appendix)

$$\Gamma = t_{adv}\left(1 + \frac{1}{\alpha}\right). \tag{7}$$

The mean transit time Γ is always greater than or equal to the advective time t_{adv} to position x, with $\Gamma \gg t_{adv}$ for $\alpha \ll 1$ (narrow currents). Counterintuitively, Γ is independent of the mixing time t_{mix} despite the fact that the TTD itself is quite sensitive to t_{mix} (Fig. 2). In the interior both the TTD and Γ depend on t_{mix} (see the appendix). To understand why Γ in the boundary current is independent of the mixing it is useful to first consider Γ in the interior. The only way the interior region gets new water is through mixing with the boundary current. If the mixing is slow, the interior region takes a long time to renew, and Γ in the interior is old. The contribution of mixing of interior water back into the boundary current is then a slow trickle of very old water. Most recent water comes directly from alongstream advection. In contrast, in the case of rapid mixing there is a shorter renewal time, and younger mean ages, in the interior region. Mixing back into the boundary current then makes a relatively larger contribution. In this model the slow trickle of old water has the same impact as the more rapid flow of younger water so that the dependence on mixing rate falls out. (Note, this is not the case if there is net divergence in the boundary current, for example, a termination of the boundary current where it merges with the interior. In this case the interior region gets renewed even in the absence of mixing.)

Unauthenticated | Downloaded 05/20/24 05:05 AM UTC

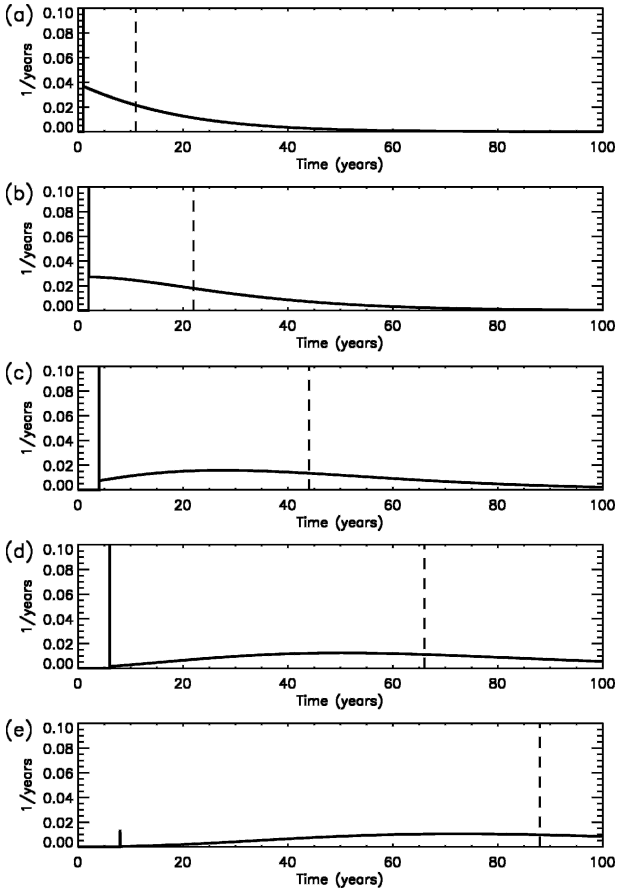

FIG. 3. TTDs at a distance x = (a) 1575, (b) 3150, (c) 6300, (d) 9450, and (e) 12 600 km downstream from source for $\alpha = 0.1$, $t_{\text{mix}} = 1$ yr, and $u = 5$ cm s^{-1} (1575 km yr^{-1}). The advective time t_{adv} to these locations is 1, 2, 4, 6, and 8 yr, respectively.

The standard deviation of the boundary current TTD at position x is

$$\sigma = \left(\frac{t_{\text{adv}} t_{\text{mix}}}{\alpha^2}\right)^{1/2}. \tag{8}$$

[The standard deviation $\sigma = \sqrt{2}\Delta$, where Δ is the "width" used by Hall and Plumb (1994) and Waugh et al. (2003).] In contrast to Γ, σ depends on the mixing time t_{mix}. Surprisingly, σ increases for slower mixing. This can be again understood by considering the contribution of mixing of interior water back into the boundary current. As discussed above, for slow mixing most of water comes via advective path with a very small amount of very old water that has been through the interior. However, this small amount makes a very large contribution to σ. In contrast for rapid mixing there is little water via advection and most water has same transit time (which is close to Γ), and the TTD is nearly symmetric about Γ with very small σ (e.g., Fig. 2d).

4. Idealized tracers

Before considering tracers with realistic (observed) boundary conditions we consider tracers with idealized boundary conditions for which analytical solutions can be obtained directly from Eqs. (3) and (4). Understanding the propagation of these idealized tracers is helpful for understanding propagation of observed tracers.

a. Exponential tracers

We first consider conserved tracers with exponential growth; that is, $\chi(0, t) = e^{t/T_{\text{exp}}}$. Such an increase is a good approximation of the change in CFCs between 1960s and late 1980s (e.g., Pickart et al. 1989). A common propagation diagnostic is the tracer age (or concentration age) τ, defined as $\chi[x, t - \tau(x)] = \chi(0, t)$. The tracer age is often taken as a measure of the time since the parcel at x was last at $x = 0$, although, as has been discussed in a number of studies (e.g., Waugh et al. 2003), and as we will see below, this interpretation is often not straightforward. Note that the tracer age, τ_{exp}, of a conserved tracer with exponential growth yields the same age as a radioactive tracer, with constant surface concentration, that decays at the same rate (Delhez et al. 2003; Waugh et al. 2003).

For exponentially increasing tracers analytical solutions for the tracer age can be obtained from Eqs. (3) and (4) (see the appendix)

$$\tau_{\text{exp}} = t_{\text{adv}}\left(1 + \frac{1}{\alpha + r_{\text{exp}}}\right), \tag{9}$$

where $r_{\text{exp}} = t_{\text{mix}}/T_{\text{exp}}$. This expression shows that the tracer age is bounded by the advective time, $t_{\text{adv}} = x/u$, and the mean transit time; that is, $t_{\text{adv}} \leq \tau_{\text{exp}} \leq \Gamma$. [The tracer age of an exponentially increasing tracers is less than the mean transit time is a general result that holds for all flows (Delhez et al. 2003; Waugh et al. 2003).] Furthermore, for fixed geometry (α) the ratio of tracer age to advective time depends only on r_{exp}. An expression of the ratio age of two tracers with different exponential growth rates can also be derived, for example, Pickart et al. (1989), but we focus here on concentration ages.

Consider first the limits of large and small r_{exp}. If the mixing time is much longer than the time scale for tracer growth ($r_{\text{exp}} \gg 1$) then Eq. (9) reduces to $\tau_{\text{exp}} \approx t_{\text{adv}}$; that is, the tracer age within the boundary current equals the advective time, independent of the tracer growth rate. In this limit new tracer is advected along the boundary current core before mixing with the interior can have any appreciable impact, and the tracer propagation approximates simple bulk advection. In the other limit, $r_{\text{exp}} \ll \alpha$, Eq. (9) becomes

Unauthenticated | Downloaded 05/20/24 05:05 AM UTC

$\tau_{exp} \approx t_{adv}(1 + 1/\alpha) = \Gamma$. Thus, in the limit of very rapid mixing the tracer age equals the mean transit time (which is much larger than the advective time, for narrow boundary currents), and again there is little sensitivity of the tracer age to the tracer growth rate. In the limit of rapid mixing the TTDs are nearly symmetrical with a relatively narrow peak at the mean transit time (e.g., Fig. 2d).

We now consider mixing rates between these two limits. Figure 4 shows the variation of tracer age with mixing time t_{mix}, for several different values of T_{exp} (as in Fig. 2, $\alpha = 0.1$). In the high and low t_{mix} limits all tracer ages collapse to t_{adv} and Γ, respectively, as discussed above. In between these limits, however, the tracer age varies strongly with time scale for tracer growth. For example, for $t_{mix} = 1$ yr the age of a tracer with $T_{exp} = 7$ yr (approximately the growth time scale of CFC113 from 1960s to 1980s) is around 5 times the advective time, whereas the age is around 9 times the advective time for $T_{exp} = 30$ yr (approximate time scale for CCl_4). The variation of age with mixing and tracer growth for different α is very similar to that shown in Fig. 4. For smaller α there are older tracer ages, especially for weak mixing when the tracer ages tend to the mean transit time, which is proportional to $(1 + 1/\alpha)$.

As discussed in the introduction the variation of tracer ages with distance has been used to estimate a spreading rate. From Eq. (9) we have that the spreading rate of the age of an exponentially increasing tracer is

$$v_{exp} = \frac{\partial x}{\partial \tau_{exp}} = \left(\frac{\alpha + r_{exp}}{1 + \alpha + r_{exp}}\right)u.$$

This shows that (for finite t_{mix}) the tracer spreading rate is less than the core speed, $v_{exp} \leq u$. Also, the tracer spreading rate decreases with increasing r_{exp}. This is illustrated in the upper curves in Fig. 5a, which show the variation of tracer age with x for several T_{exp} with $\alpha = 0.1$, $u = 5$ cm s^{-1}, and $t_{mix} = 1$ yr. For $t_{mix} = 1$ yr (and measurements in 1990s) the spreading rates of CFC113 and CCl_4 are around $u/5$ and $u/9$, with CFC11 and CFC12 spreading rates between these values.

b. Periodic tracers

Temporal variations (anomalies) in temperature and salinity on decadal and shorter time scales have been observed superposed on longer-term trends in the subpolar and polar North Atlantic. The propagation of these anomalies has been used to estimate transport time scales and spreading rates in the DWBC (e.g., Molinari et al. 1998; Freudenthal and Andrie 2002; Stramma et al. 2004). Such anomalies constitute tracers distinct from the steady increase of CFCs (between the 1960s and 1990s). To understand differences between the propagation of these two types of tracers it is useful to consider idealized tracers with periodic boundary conditions, and to contrast them with the exponentially increasing tracers.

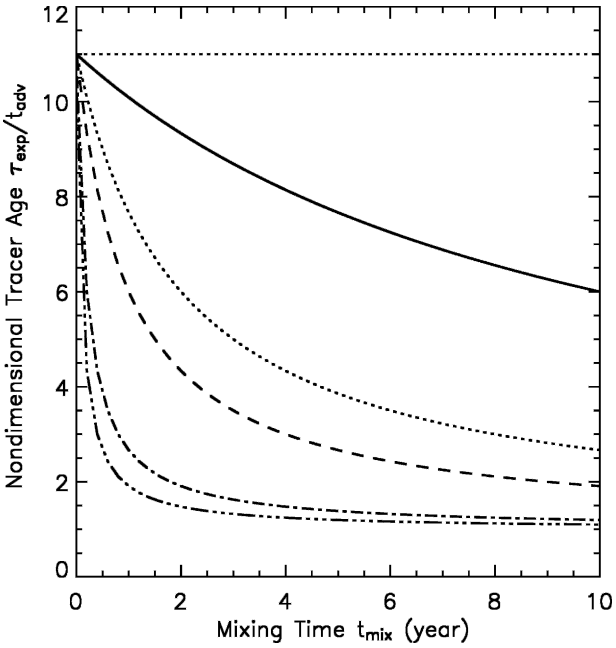

FIG. 4. Variation of ratio of age of exponential tracer to advective time τ_{exp}/t_{adv} with mixing time t_{mix} for tracer growth time T_{exp} = 100 (solid curve), 20 (dotted), 10 (dashed), 5 (dot–dashed), and 1 yr (triple dot–dashed). The horizontal dotted line shows the mean transit time Γ.

For tracers with periodic boundary condition, that is, $\chi(0, t) = \mathrm{Re}(e^{i2\pi t/T_\omega})$, the propagation time of the phase of the signal (or "phase lag") τ_ω and the relative amplitude A_ω are (see the appendix)

$$\tau_\omega = t_{adv}\left[\frac{\alpha(\alpha + 1) + r_\omega^2}{\alpha^2 + r_\omega^2}\right] \quad \text{and} \tag{10}$$

$$A_\omega = \exp\left[\frac{-t_{adv}r_\omega^2}{t_{mix}(\alpha^2 + r_\omega^2)}\right] = \exp\left(\frac{-x}{L}\right), \tag{11}$$

where $r_\omega = 2\pi t_{mix}/T_\omega$ is the ratio of the time scales for mixing and tracer variations, and $L = ut_{mix}(\alpha^2 + r_\omega^2)/r_\omega^2$ is the decay length scale of the amplitude. As with age of exponential tracers, the phase lag is bounded by the advective time scale t_{adv} and the mean transit time Γ, and the ratio of tracer time scale to advective time depends (for fixed α) only on the ratio of time scales for tracer variations and mixing.

If the period of the tracer variation is much shorter than the mixing time, $r_\omega \gg 1$, then Eqs. (10) and (11)

Unauthenticated | Downloaded 05/20/24 05:05 AM UTC

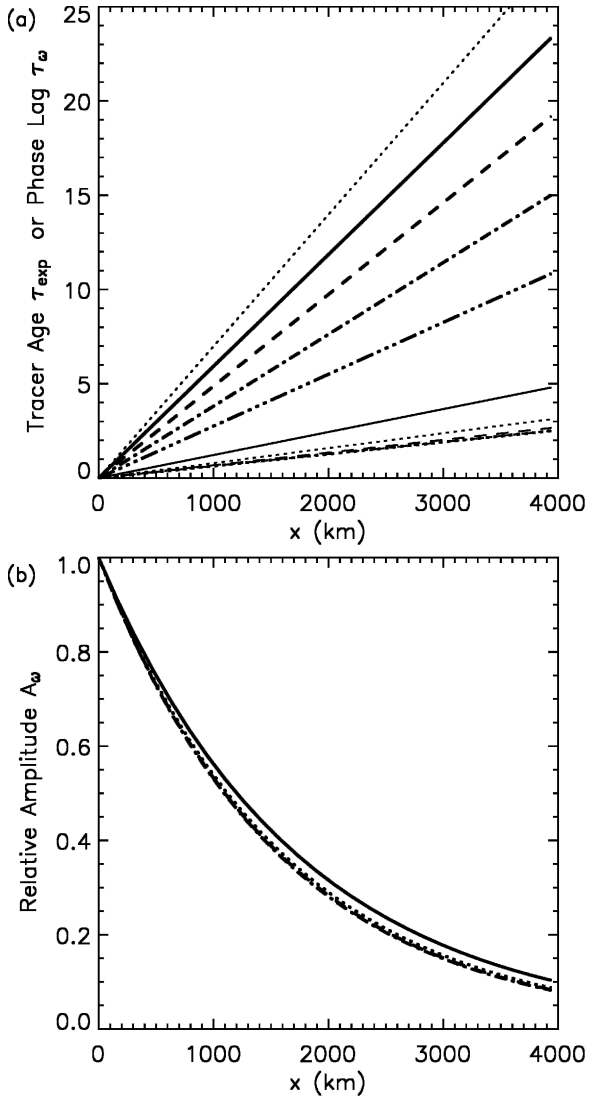

FIG. 5. Variation of (a) mean transit time Γ, age of exponential tracer τ_{exp}, and phase lag of periodic tracer τ_ω and (b) amplitude of period tracer A_ω with x for $\alpha = 0.1$, $u = 5$ cm s^{-1}, and mixing time $t_{mix} = 1.0$ yr. The upper set of curves in (a) show Γ (dotted curve) and tracer age with $T_{exp} = 50$ (solid curve), 20 (dashed), 10 (dot–dashed), and 5 (triple dot–dashed) yr, whereas the lower set of curves show the phase lag for $T_\omega = 20$ (solid), 10 (dotted), 5 (dashed), and 1 (dot–dashed) yr.

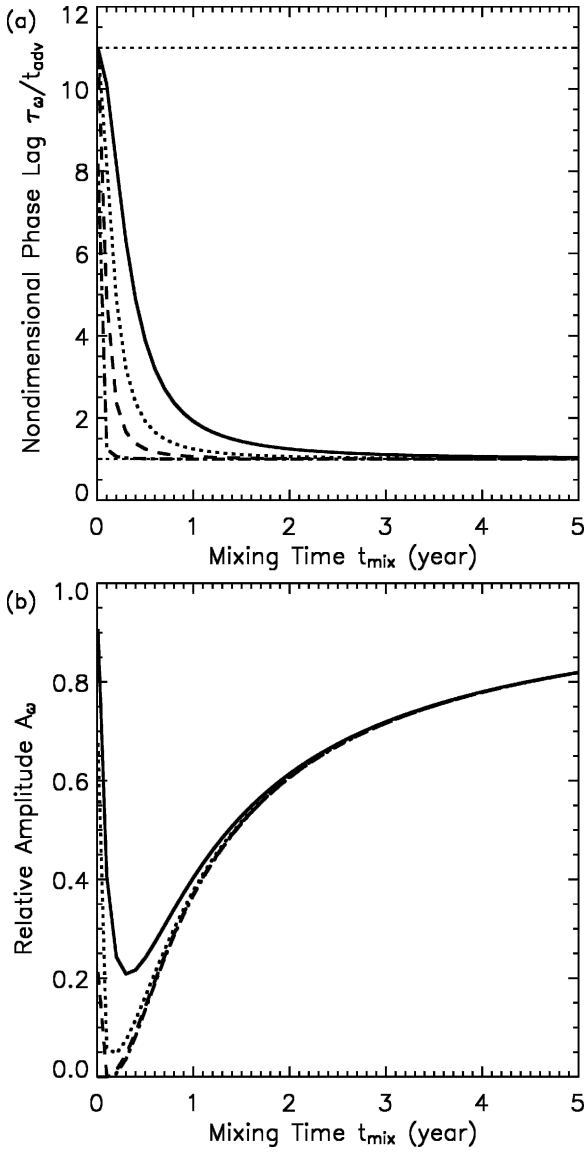

FIG. 6. Variation of (a) phase lag τ_ω and (b) amplitude A_ω of periodic tracers with mixing time t_{mix} for periods equal to 20 (solid), 10 (dotted), 5 (dashed), and 1 (dot–dashed) yr. In both plots $\alpha = 0.1$ and $t_{adv} = 1$ yr.

reduce to $\tau_\omega \approx t_{adv}$ and $A_\omega \approx \exp(-t_{adv}/t_{mix})$ (or $L \approx ut_{mix}$). That is, the tracer signal propagates at the advective speed and the amplitude attenuates over a length scale equal to ut_{mix}. TTDs in this limit can still be broad with long tails (see Figs. 2c,d), but this tail contributes little to the phase lag. The tail encompasses several complete tracer cycles at roughly equal magnitude, which cancel, and the net signal is due solely to the advective peak. In fact, in this limit, the amplitude of the tracer is equivalent to $\hat{G}_1$, the magnitude of the advective spike of the TTD [see Eq. (6)].

In the opposite limit $r_\omega \ll \alpha$, the Eqs. (10) and (11) reduce to $\tau_\omega \approx t_{adv}(1 + 1/\alpha) = \Gamma$ and $A_\omega \approx 1$ (or $L = \infty$). That is, when the tracer period is much greater than the mixing time scale, the tracer time lag equals the mean transit time and the amplitude is conserved.

Figure 6 shows the variation of the phase lag and amplitude with mixing time for several different tracer periods T_ω (again with $t_{adv} = 1$ yr and $\alpha = 0.1$). Consistent with the above analysis, for $t_{mix} > 1$ there is little

Unauthenticated | Downloaded 05/20/24 05:05 AM UTC

sensitivity of the phase lag or amplitude to the period of the tracers. For smaller t_{mix} there is some sensitivity, particularly for tracers with periods greater than 10 yr. However, for t_{mix} around 1 yr and tracers with periods around or less than 10 yr there is only weak sensitivity, with the phase lag being close to the advective time. Thus, in this regime, the tracer signal downstream of the source will have the same temporal variations as at the source except lagged by the advective time and smaller amplitude. The weak sensitivity of the phase lag and amplitude to the frequency of the tracer variation means that the propagation of tracer signals is nondispersive.

Figures 5b and 6b show that for moderate and large mixing there is rapid attenuation of the amplitude of periodic tracers. For example, for the parameters in Fig. 5b the attenuation length scale, L, of the amplitude is around 2000 km, and the amplitude at $x = 4000$ km is less than 10% of that at the source and is less than 2% at $x = 6000$ km.

This analysis of the variations of the phase lag and amplitude of periodic tracers suggests that, within the intermediate mixing regime, decadal or shorter variations in temperature or salinity (or other other tracers) propagate at roughly the advective speed, which is much faster than the propagation of steadily growing (or decaying) transient tracers, such as CFCs. Furthermore, the amplitude of these variations attenuate rapidly with distance.

5. Realistic tracers

The above analysis of idealized tracers shows that in the simple boundary current model large differences can exist among the time scales inferred from different tracers. As discussed in the introduction, differences in tracer time scale (spreading rates) have indeed been noted from observations. To examine this in more detail we now consider the evolution of realistic tracers in the model.

a. Transient tracers

We first consider the distributions of transient tracers CFCs, SF_6, and tritium (^3H) and daughter product helium-3 (^3He). The concentrations and ages of these tracers are determined using Eqs. (3) and (4) together with specified boundary conditions $\chi(0, t)$. For CFCs and SF_6 boundary conditions we use their atmospheric histories (Walker et al. 2000; Maiss and Brenninkmeijer 1998) scaled to 70% of the equilibrium solubility. This represents typical source conditions of North Atlantic overflow waters (Smethie et al. 2000; Smethie and Fine 2001). For tritium the Denmark Strait overflow water (DSOW) time series from Doney and Jenkins (1994) is used as the boundary condition, and a decay rate $\lambda = 0.055\ 76\ yr^{-1}$ is used in Eq. (3). The helium-3 concentration is then calculated as the concentration of tritium lost through radioactive decay. (We neglect small mantle helium-3 sources from seafloor vents.) The tritium and helium concentrations are then combined together to form a tritium–helium age, defined as in Jenkins and Clarke (1976).

We first compare model distributions of these transient tracers with observations along the North Atlantic DWBC. The symbols in Fig. 7 show the observed variations of tritium concentration (Fig. 7a) and tritium-helium age (Fig. 7b) in 1981 (Doney and Jenkins 1994), and CFC11 concentration age (Fig. 7c) and CFC11/CFC12 ratio age (Fig. 7d) in 1991 (Smethie et al. 2000). These observations show that the tritium concentration decreases and tracer ages increase with distance along the DWBC, and that the CFC11 concentration age is significantly older than the tritium–helium age and CFC11/CFC12 ratio age at the same location. (As the CFC11/CFC12 ratio peaked in the mid-1980s the ratio age cannot be defined for the "younger" water in 1991.) The curves in Fig. 7 show model calculations for $u = 5$ cm s^{-1}, $\alpha = 0.1$, and several values of t_{mix}. For $t_{mix} \approx 1$ yr the model reproduces well the observed variations in all four quantities. Thus, despite its great simplicity, the model is surprisingly good at reproducing the observed tracer signals. Note that, consistent with previous analysis (e.g., Delhez et al. 2003; Waugh et al. 2003), the ages from all tracers are less than the mean age (Fig. 5a).

Equally good fits to all four observed quantities are obtained for other values of α, u, and t_{mix}, but the range of values is relatively small. For $\alpha = 0.05$ the data are fit for u around 7–9 cm s^{-1} and t_{mix} between 1.5 and 0.5 yr (for slower advection a longer mixing time is required to match the data), whereas for $\alpha = 0.15$ the data are fit for u around 3–5 cm s^{-1} and t_{mix} between 1.5 and 0.5 yr. For smaller or larger α it is not possible to match all four quantities simultaneously. The above range of values for u, t_{mix}, and α that result in good agreement between model and observations lies within the "intermediate mixing" regime in which the CFC and ^3He tracer ages lie between the advective time scale t_{adv} and the mean transit time Γ.

The values for both u and t_{mix} are similar to best-fit values in the models of Pickart et al. (1989) and Doney and Jenkins (1994). Furthermore, the model core velocity in this parameter range ($u \approx 5$ cm s^{-1}) is also similar to mean velocities from direct measurements (e.g., Watts 1991; Pickart and Smethie 1998). For the

Unauthenticated | Downloaded 05/20/24 05:05 AM UTC

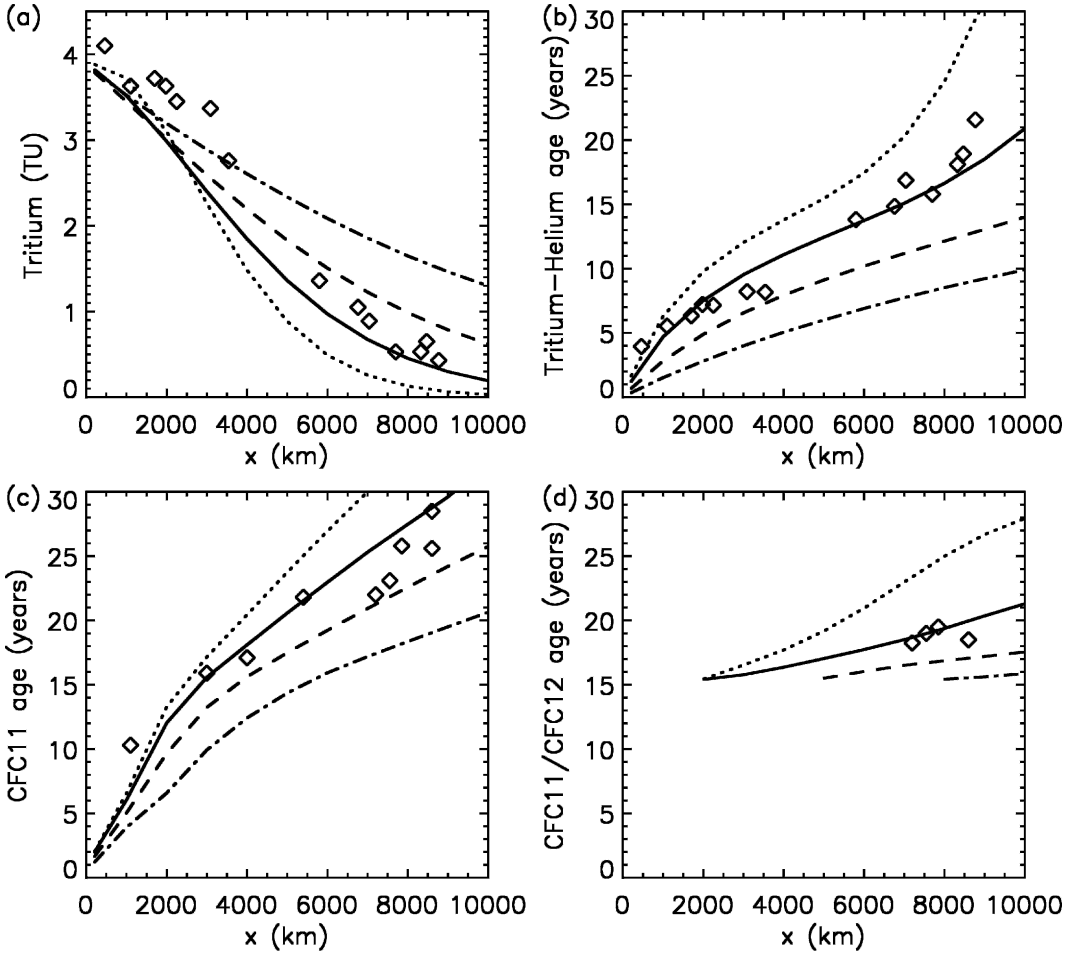

FIG. 7. Variation of (a) tritium, (b) tritium–helium age, (c) CFC11 concentration age, and (d) CFC11/CFC12 ratio age with x for $t_{mix} = 4$ (dot–dashed), 2 (dashed), 1 (solid), and 0.5 (dotted) yr. In these calculations $\alpha = 0.1$ and $u = 5$ cm s^{-1} (1575 km yr^{-1}). Tritium concentrations and ages are for 1981, wheras CFC ages are for 1991. Symbols are data from (a), (b) Doney and Jenkins (1994) or (c), (d) Smethie et al. (2000). See text for details.

reasons discussed in section 4, however, $u = 5$ cm s^{-1} is significantly larger than the tracer-age spreading rates.

We now examine modeled tracer ages in the same mixing regime for a larger suite of tracers. Figure 8 shows the spatial dependence of tracer age (in 1991) for CFC11, CFC12, CFC113, tritium–helium, CCl_4, and SF_6. The model parameter values are $u = 5$ cm s^{-1}, $t_{mix} = 1$ yr, and $\alpha = 0.1$. The CFC11, CFC12 and tritium–helium ages are similar, except for x greater than about 5000 km where the tritium–helium age is several years younger than CFC11 and CFC12 ages. The CFC-113 and SF_6 ages are similar to each other, but are younger than CFC11, CFC12, and tritium–helium ages. On the other hand, the CCl_4 age is older than all the other tracers shown. These relationships among the tracer ages hold for other parameters values in the intermediate mixing regime and are consistent with our analysis of exponentially growing tracers (e.g., Fig. 4).

The range of tracer ages in Fig. 8 is broadly consistent with measurements made in the 1990s of CFCs (Azetsu-Scott et al. 2003) and tritium and helium (Khatiwala et al. 2002) in DSOW within the Labrador Sea. Calculations of ages from these observations yield CFC113 ages around 10 yr, tritium–helium, CFC11, and CFC12 ages around 15 yr, and CCl_4 ages around 20 yr These ages are in reasonable agreement with Fig. 8 for $x = 2500$ km, the approximate distance from Denmark Strait to the Labrador Sea.

b. Hydrographic tracers

We now consider the propagation of temperature and salinity anomalies. These anomalies act as tracers with fluctuating boundary conditions, and the model analysis of section 4b shows that fluctuating tracers with period less than about 10 yr have a time scale for phase propagation closely approximating the advective time

Unauthenticated | Downloaded 05/20/24 05:05 AM UTC

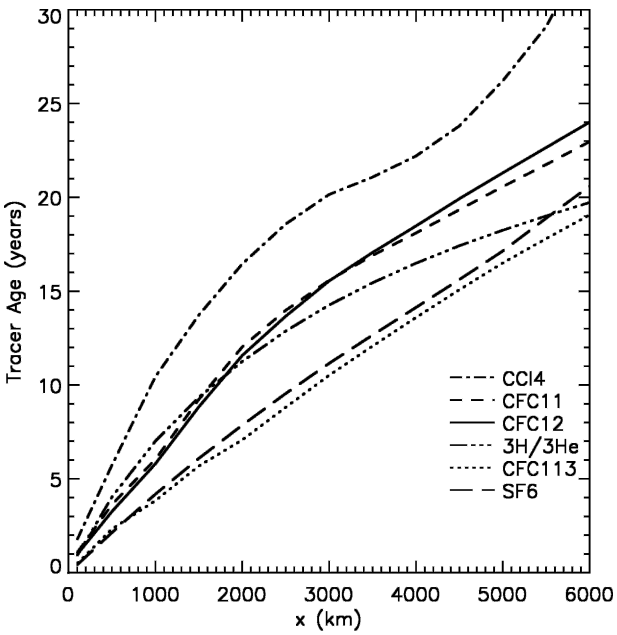

FIG. 8. Variation of SF_6 (long-dashed), CFC113 (dotted), tritium–helium (triple dot–dashed), CFC12 (solid) CFC11 (dashed), and CCl_4 (dot–dashed) tracer ages (in 1991) with distance x, for $t_{mix} = 1$ yr, $\alpha = 0.1$, and $u = 5$ cm s^{-1}.

for flow in the intermediate-mixing regime. We therefore expect anomalies in T and S to propagate more quickly along the boundary current than would be indicated by a simple interpretation of CFC or tritium–helium age.

Dickson et al. (2002) presented salinity time series of overflow waters in the Irminger and Labrador Seas. The major focus of their analysis was the long-term freshening of these waters, but the data also show more rapid variations (oscillations) about this long-term trend. These variations propagate from overflow sills to the Labrador Sea in less than 2 years. For example, the minimum in DSOW salinity at Denmark Strait in 1994 is observed at the western Irminger Sea in 1995 and in the Labrador Sea in 1996. A 2-yr spreading time is consistent with the simple DWBC model: It is much shorter than the typical tracer ages in the Labrador Sea of 10 and 20 yr (see above) and implies an anomaly spreading rate around 4 cm s^{-1}, which is close to the mean current speed. Rapid spreading of DSOW temperature anomalies was also observed by Stramma et al. (2004). They noted a propagation time of less than 2 yr between the Labrador Sea (56°N) and Grand Banks (43°N), which implies a lower bound on the spreading rate of 3–4 cm s^{-1}. This is again broadly consistent with the model.

Temporal variations in temperature and salinity within the subtropical and tropical DWBC have also been reported: for example, Molinari et al. (1998) and Freudenthal and Andrie (2002). These studies calculated spreading rates based on anomalies in LSW within the DWBC that are faster than those calculated from tracer ages (2–2.5 cm s^{-1} as compared with 1–2 cm s^{-1}). While this difference between hydrographic anomalies and transient tracer ages is qualitatively consistent with the model, there are quantitative differences for intermediate-mixing parameters. The model-predicted transit time (the advective time) is much shorter than that inferred from the hydrographic observations: assuming a mean current speed of 5 cm s^{-1} the time for advection over 6000 km (Labrador Sea to the subtropics) is around 4 years, whereas the above studies infer transit times of 8–10 years. Furthermore the model predicts that the amplitude of the anomalies should be extremely small (e.g., assuming $u = 5$ cm s^{-1} and $t_{mix} = 1$ yr the amplitude 6000 km downstream from the source is only about 2% that at the source), whereas the observed tropical anomalies are of similar amplitude to those in the Labrador Sea.

It is possible that these model–data differences are due to the simplicity of the model. However, as shown in the next section, the above conclusions regarding the propagation and decay of periodic tracer signals are robust to inclusion of addition processes in the model. An alternative possibility is that the observed T and S anomalies in the subtropical and tropical DWBC are not simply transported versions of subpolar anomalies, but instead are generated (partially or totally) by temporal variations in DWBC transport acting on background gradients. For example, the dynamical variability that produce the T and S anomalies may also affect the transport pathways or generate waves that alter T and S in the Tropics (e.g., Yang and Joyce 2003; Johnson and Marshall 2002). Another possibility is that the observed LSW anomalies could be due to local transport features—for example, eddies.

6. Discussion

The analysis above has shown that the DWBC model matches the observed tracer variations in the intermediate-mixing regime (i.e., mixing time comparable to advective time), and in this regime tracer ages are sensitive to the nature and details of the tracer history at the source region. In particular, the spreading time of periodic tracers with decadal variations (e.g., anomalies in T and S) is much shorter than CFC or tritium–helium ages, which are in turn much younger than the mean age. Moreover, the amplitude of these decadal oscillations is rapidly attenuated with distance, having an e-folding scale about 2000 km. Given the great simplicity

Unauthenticated | Downloaded 05/20/24 05:05 AM UTC

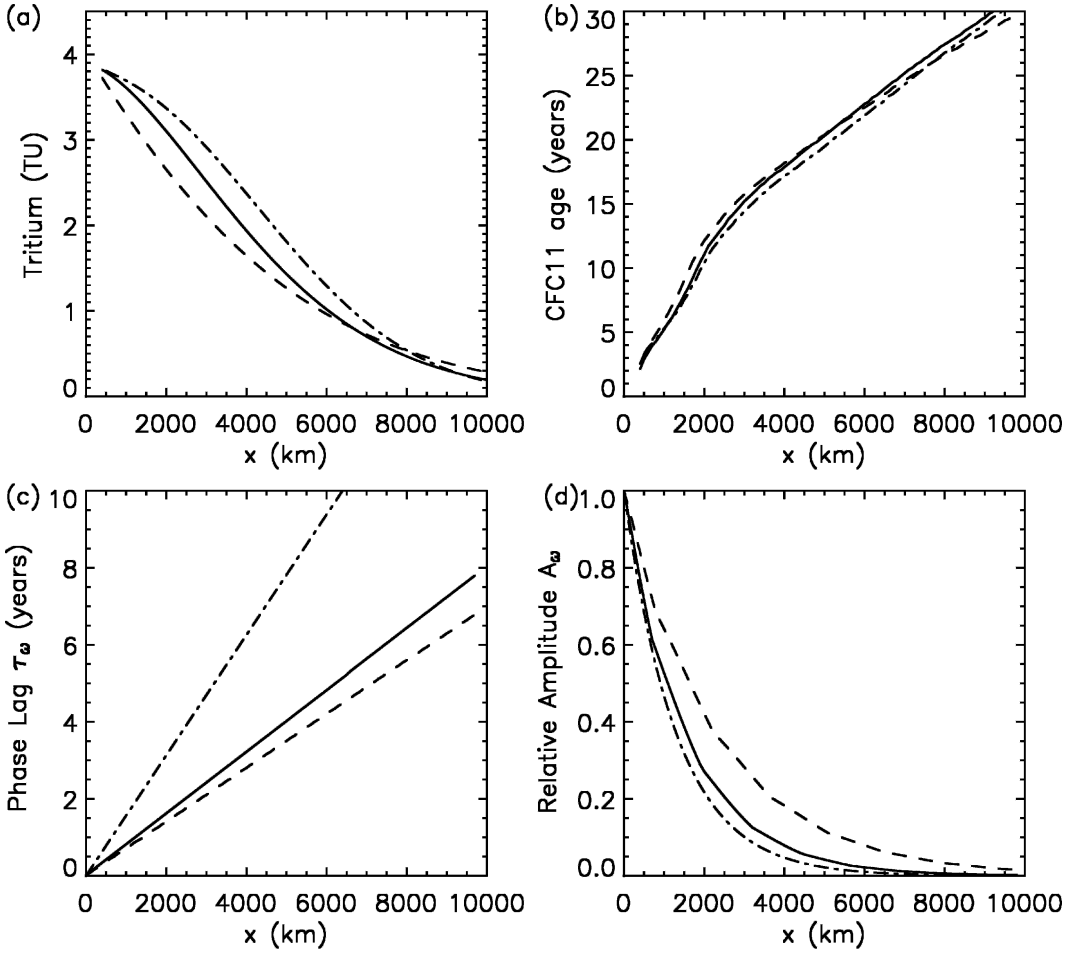

FIG. 9. Variation with distance x of (a) tritium (in 1981), (b) CFC11 concentration age (in 1991), and (c) phase lag and (d) amplitude of tracer with 10-yr period for ID advection–diffusion with $u = 5$ cm s^{-1} and $\kappa = 10\,000$ m^2 s^{-1} (dot–dashed) and for DWBC model with no interior flow (solid) or with flow $u_i = -\alpha u_b$ in the interior region (dashed). In the DWBC model calculations $\alpha = 0.1$, $u = 5$ cm s^{-1}, and $t_{\text{mix}} = 1$ yr in calculation with no interior flow and $t_{\text{mix}} = 1.5$ yr with interior flow.

of the model it is reasonable to ask how robust these conclusions are. To investigate this we use a numerical version of the DWBC model in order to relax some of the simplifications made in the analytical solutions, and also examine a 1D advection–diffusion model.

For 1D advection–diffusion with constant coefficients analytical solutions are available for the TTD and exponential and periodic tracers (e.g., Hall and Plumb 1994). For coefficient values of velocity $u \approx 0.5$ cm s^{-1} and diffusivity $\kappa \approx 10\,000$ m^2 s^{-1} the 1D model matches the tracer data as accurately as the DWBC model. For example, Figs. 9a and 9b compare the CFC11 age and tritium concentration for 1D advective–diffusive flow with the above parameters with the same fields for the analytic DWBC with $u = 5$ cm s^{-1} and $t_{\text{mix}} = 1$ yr. Similar agreement is also found for exponentially increasing tracers with a wide range of growth rates (not shown). For the two models to produce similar tracer distributions, the advective velocity u in the 1D model must be much smaller than that in the DWBC model. This is because in the 1D model the large along-flow diffusion contributes to the tracer propagation. Note, however, that, although the velocities in the two models differ by an order of magnitude, in both cases the advective time is comparable to the diffusive time; that is, both models are in intermediate-mixing regimes.

There are some differences in the propagation of periodic tracers between the DWBC and 1D models when parameters in both models are chosen to match the tracer data. The phase lag time of decadal or shorter oscillations in the 1D model is greater, the amplitude is attenuated more rapidly, and there is higher sensitivity to the tracer period, as shown in Figs. 9c and 9d. Con-

Unauthenticated | Downloaded 05/20/24 05:05 AM UTC

sequently, the difference between periodic and exponential tracers is smaller in the 1D model than in the DWBC model. However, even in the 1D model the phase lag time of decadal variations is less than the CFC11 age by a factor of 3. Hence, the result in the DWBC model that decadal variations in T and S propagate much more quickly than spreading rates from CFC or tritium–helium ages and are rapidly attenuated are corroborated by the 1D advection–diffusion model.

As a further test of the results from the analytical DWBC model we relax the simplifications of the reduced Eqs. (3) and (4) by adding realistic along-flow diffusion and having the interior region advect an amount that balances the water mass flux of the boundary region ($u_i = -\alpha u_b$). We are no longer able to obtain analytical solutions for the TTD and tracers, but solving the equations numerically is straightforward. [To minimize numerical diffusion during advection we employ the second-order moments algorithm of Prather (1986).]

Typical values of isopycnal diffusivity are $O(1000\ \mathrm{m^2\ s^{-1}})$ (e.g., Ledwell et al. 1998). However, adding along-flow diffusion as large as $10\,000\ \mathrm{m^2\ s^{-1}}$ to the boundary current region makes negligible difference to the tracer distributions, and the CFC, tritium, and periodic-tracer curves are indistinguishable from the zero-diffusion curves in Fig. 9. The minimal impact of realistic levels of diffusion is consistent with the scaling argument of section 2. Along-flow diffusion does not affect our conclusions about relative propagation rates of tracers.

Last, we consider the case in which there is a return flow in the interior region, $u_i = -\alpha u_b$, so that mass continuity is satisfied. Now, the mixing time scale that gives close agreement to the CFC and tritium data is slightly larger $t_{\mathrm{mix}} = 1.5$ yr, with u and α unchanged (Figs. 9a,b). The increased isolation compensates the tendency for the return flow of the interior to supply older, more tracer-depleted water to the boundary region. The amplitude of the 10-yr periodic tracer (Fig. 9b) is now somewhat less attenuated because of the increased isolation. Nonetheless, these parameter values still put the model well in the intermediate mixing regime. The phase-lag time changes little and is still much smaller than the CFC and tritium ages (Fig. 9c). Hence, the inclusion of a flow in the interior region does not change the main conclusion concerning the relative propagation of tracer signals.

7. Conclusions

We have examined the transit-time distribution and the propagation of transient tracers along the DWBC using a simple model composed of a narrow advective core mixing with a larger surrounding region, representing the ocean interior. In the limit of either very rapid or very slow mixing between the current and interior region there is only weak sensitivity of tracer propagation times (tracer ages) to the tracer's concentration history at the source region. Between these mixing limits, however, tracer ages are sensitive to the concentration history at the source. The tracer age of tracers with exponentially increasing and periodic histories ranges from a simple bulk advective transit time to the much larger mean transit time, depending on the ratio of the tracer time scale (exponential time constant or period of fluctuation) to the mixing time.

Comparisons of the model with CFC, tritium, and helium observations indicate that the North Atlantic DWBC is in the intermediate mixing regime, with current speed $u \approx 5\ \mathrm{cm\ s^{-1}}$ and mixing time $t_{\mathrm{mix}} \approx 1$ yr. A current speed of $5\ \mathrm{cm\ s^{-1}}$ is similar to the mean velocities from direct measurements (e.g., Watts 1991; Pickart and Smethie 1998) as well as the values obtained by Pickart et al. (1989) and Doney and Jenkins (1994) for their models. This velocity, however, is faster than spreading rates inferred from CFC and tritium–helium ages, which are around 1–2 $\mathrm{cm\ s^{-1}}$. For these parameter values the phase of periodic tracers with decadal or shorter periods will propagate at roughly the current speed, and the amplitude of these variations will decay with an e-folding length scale of about 2000 km. This implies that decadal or shorter fluctuations in hydrographic tracers (temperature or salinity) propagate much more quickly than the spreading rate inferred from CFC or tritium–helium ages, and that in the Tropics the signal amplitude of such variations is only ~2% of the subpolar source amplitude.

These conclusions are robust to variations of the details of the model. Fluid flow, or lack thereof, in the interior region has only weak impact on tracer distributions in the boundary current region, while realistic levels of along-flow diffusion has a negligible impact. Furthermore, an alternate 1D advective–diffusive model tuned to the same DWBC CFC and tritium observations produces qualitatively similar results for periodic tracers; namely, periodic tracer signals propagate more rapidly than the spreading indicated by CFC and tritium ages, and the amplitude attenuates by several e-folds from subpolar to tropical regions.

The observed propagation of fluctuations in DSOW salinity and temperature in the North Atlantic DWBC are broadly consistent with these model predictions. DSOW salinity anomalies are observed to take less than 2 years to propagate from Denmark Strait to the Labrador Sea (Dickson et al. 2002) while DSOW temperature anomalies are observed to propagate from the

Unauthenticated | Downloaded 05/20/24 05:05 AM UTC

56° and 43°N in less than 2 years (Stramma et al. 2004). Both observations imply spreading rates of at least 3–4 cm s^{-1}, more rapid than spreading rates from tracer ages and close to the observed mean current speed. However, transit times inferred from LSW anomalies measured in the (sub) tropical Atlantic (e.g., Molinari et al. 1998; Freudenthal and Andrie 2002) are around twice that predicted, assuming a current speed of 5 cm s^{-1}, and the tropical anomalies have much greater amplitude than predicted by the model. The cause for these differences is unclear. They could be due to deficiencies in the simple model. It is also possible that the anomalies observed in the Tropics are not simply transported subpolar anomalies. Preliminary analysis suggests that periodicity in transport acting on background gradients can produce tracer oscillations locally with amplitudes larger than tracer signals propagated from remote regions. However, further work is needed to examine these issues.

A general conclusion from this study is that the impact of mixing on the spreading rate of tracer signals in DWBCs varies among tracers, and a wide range of spreading rates can be obtained. This indicates that the tracers contain independent information and suggests that tight constraints on the flow and transport in DWBCs can be obtained from simultaneous measurements of several different tracers, in particular hydrographic anomalies and steadily increasing transient tracers. One approach for such an analysis is to perform a more detailed model–observation comparison than presented here, including the large database of tracer measurements that now exists from the World Ocean Circulation Experiment and other programs. Another approach is to use measurements to constrain aspects (e.g., moments) of the TTDs, without direct reference to a particular transport model. Klatt et al. (2002) and Steinfeldt and Rhein (2004) have performed such an analysis, using repeat CFC measurements to infer the TTDs in the Weddell Sea and tropical Atlantic DWBCs. We plan to explore both approaches in the future.

Acknowledgments. We thank Tom Haine and Toste Tanhua for useful discussions and comments, and Bill Smethie for providing the CFC data shown in Fig. 7. This work was supported by the National Science Foundation and the National Oceanic and Atmospheric Administration. TMH acknowledges support from the National Aeronautics and Space Administration.

APPENDIX

Full Solutions

The transit-time distributions, mean transit time, ages of exponentially increasing tracers, and phase and amplitude of periodic tracers for the model are determined by solving Eqs. (3) and (4) with different sources S and boundary condition $\chi_b(0, t)$.

The TTDs $\mathcal{G}_b$ and $\mathcal{G}_i$ are the solutions of Eqs. (3) and (4) with $S_b = S_i = 0$ and $\chi_b(0, t) = \delta(t)$. These solutions are found by taking the Laplace transform of Eqs. (3) and (4) and then solving a first-order differential equation for the Laplace transform of $\mathcal{G}_i$. This yields

$$\mathcal{G}_b(x, t) = \hat{G}_1\delta(t - t_{\text{adv}}) + \hat{G}_2\Theta(t - t_{\text{adv}}) \quad \text{and}$$

$$\mathcal{G}_i(x, t) = \hat{G}_3\Theta(t - t_{\text{adv}}),$$

where

$$\hat{G}_1 = e^{-1/p}, \quad \hat{G}_2 = \frac{\alpha}{\zeta t_{\text{mix}}} e^{-(1+\zeta^2)/P} I_1(2\zeta/P),$$

$$\hat{G}_3 = \frac{\alpha}{t_{\text{mix}}} e^{-(1+\zeta^2)/P} I_0(2\zeta/P),$$

$t_{\text{adv}} = x/u$, $P = t_{\text{mix}}/t_{\text{adv}}$, $\zeta^2 = \alpha(\hat{t} - 1)$, $\hat{t} = t/t_{\text{adv}}$, I_0 and I_1 are modified Bessel function of zeroth and first order, δ is Dirac delta function, and Θ is the Heaviside function.

The mean transit time (mean age) of the TTDs is equivalent to the distribution of the ideal age tracer (Hall and Haine 2002). The ideal age tracer is the steady state solution of Eqs. (3) and (4) with $S_b = S_i =$ 1 yr yr^{-1} and $\chi_b(0, t) = 0$:

$$\Gamma_b = t_{\text{adv}}\left(1 + \frac{1}{\alpha}\right) \quad \text{and} \quad \Gamma_i = \Gamma_b + \frac{t_{\text{mix}}}{\alpha}.$$

For conserved tracers with exponential growth, that is, $S_b = S_i = 0$ and $\chi_b(0, t) = e^{t/T_{\text{exp}}}$, the concentrations are found using the method of separation of variables. The solutions are then combined with the definition of the tracer concentration age τ, $\chi_b(0, t - \tau) = \chi(x, t)$, to yield

$$\tau_b = t_{\text{adv}}\left(1 + \frac{1}{\alpha + r_{\text{exp}}}\right) \quad \text{and} \quad \tau_i = \tau_b + T_{\text{exp}} \ln\left(1 + \frac{r_{\text{exp}}}{\alpha}\right),$$

where $r_{\text{exp}} = t_{\text{mix}}/T_{\text{exp}}$ is the ratio of mixing to tracer growth time scales.

The solution for conserved tracers with periodic boundary conditions; that is, $\chi(0, t) = \text{Re}(e^{i2\pi t/T_\omega})$, is found in a similar manner. From these solutions it is possible to derive the time lag in phase τ_ω and amplitude A_ω at locations away from the boundary. These are

$$\tau_{\omega b} = t_{\text{adv}}\left[\frac{\alpha(\alpha + 1) + r_\omega^2}{a^2 + r_\omega^2}\right], \quad A_{\omega b} = \exp\left(\frac{-\sigma t_{\text{adv}} r_\omega^2}{a^2 + r_\omega^2}\right),$$

$$\tau_{\omega i} = \tau_{\omega b} + \frac{1}{\omega}\text{atan}\left(\frac{r_\omega}{\alpha}\right), \quad \text{and} \quad A_{\omega i} = \frac{\alpha}{\sqrt{\alpha^2 + r_\omega^2}} A_{\omega b},$$

where $r_\omega = 2\pi t_{\text{mix}}/T_\omega$ is the ratio of the time scales for mixing and tracer variations.

Unauthenticated | Downloaded 05/20/24 05:05 AM UTC

REFERENCES

Azetsu-Scott, K., E. P. Jones, I. Yashayaev, and R. M. Gershey, 2003: Time series study of CFC concentrations in the Labrador Sea during deep and shallow convection regimes (1991–2000). *J. Geophys. Res.,* **108,** 3354, doi:10.1029/2002JC001317.

Beining, P., and W. Roether, 1996: Temporal evolution of CFC 11 and CFC 12 concentrations in the ocean interior. *J. Geophys. Res.,* **101,** 16 455–16 464.

Deleersnijder, E., J. Campin, and E. J. M. Delhez, 2001: The concept of age in marine modeling I. Theory and preliminary model results. *J. Mar. Sys.,* **28,** 229–267.

Delhez, E. J. M., E. Deleersnijder, A. Mouchet, and J. M. Beckers, 2003: A note on the age of radioactive tracers. *J. Mar. Sys.,* **38,** 277–286.

Dickson, B., I. Yashayaev, J. Meincke, B. Turrell, S. Dye, and J. Holfort, 2002: Rapid freshening of the deep North Atlantic Ocean over the past four decades. *Nature,* **416,** 832–837.

Doney, S. C., and W. J. Jenkins, 1994: Ventilation of the deep western boundary current and abyssal western North Atlantic: Estimates from tritium and ^{3}He distributions. *J. Phys. Oceanogr.,* **24,** 638–659.

Fine, R. A., M. Rhein, and C. Andrie, 2003: Using a CFC effective age to estimate propagation and storage of climate anomalies in the deep western North Atlantic Ocean. *Geophys. Res. Lett.,* **29,** 2227, doi:10.1029/2002GL015618.

Freudenthal, S., and C. Andrie, 2002: The arrival of a "new" Labrador Sea Water signal in the tropical Atlantic in 1996. *Geophys. Res. Lett.,* **29,** 1741–1744.

Haine, T. W. N., and T. M. Hall, 2002: A generalized transport theory: Water mass composition and age. *J. Phys. Oceanogr.,* **32,** 1932–1946.

——, A. J. Watson, M. I. Liddicoat, and R. R. Dickson, 1998: The flow of Antarctic bottom water to the southwest Indian Ocean estimated using CFCs. *J. Geophys. Res.,* **103,** 27 637–27 653.

Hall, T. M., 2000: Path histories and timescales in stratospheric transport: analysis of an idealized model. *J. Geophys. Res.,* **105,** 22 811–22 823.

——, and R. A. Plumb, 1994: Age as a diagnostic of stratospheric transport. *J. Geophys. Res.,* **99,** 1059–1070.

——, and D. W. Waugh, 2000: Stratospheric residence time and its relationship to mean age. *J. Geophys. Res.,* **105,** 6773–6782.

——, and T. W. N. Haine, 2002: A note on ocean transport diagnostics: Ideal age and the age spectrum. *J. Phys. Oceanogr.,* **32,** 1987–1991.

——, D. W. Waugh, T. W. N. Haine, P. E. Robbins, and S. Khaliwala, 2004: Reduced estimates of anthropogenic carbon in the Indian Ocean due to mixing and time-varying air–sea CO_2 disequilibrium. *Global Biogeochem. Cycles,* **18,** GB1031, doi:10.1029/2003GB002120.

Holzer, M., and T. M. Hall, 2000: Transit-time and tracer-age distributions in geophysical flows. *J. Atmos. Sci.,* **57,** 3539–3558.

Jenkins, W. J., and W. B. Clarke, 1976: The Distribution of ^{3}He in the western Atlantic Ocean. *Deep-Sea Res.,* **23,** 481–494.

Johnson, H. L., and D. P. Marshall, 2002: Localization of abrupt change in the North Atlantic thermohaline circulation. *Geophys. Res. Lett.,* **29,** 1083, doi:10.1029/2001GL014140.

Khatiwala, S., M. Visbeck, and P. Schlosser, 2001: Age tracers in an ocean GCM. *Deep-Sea Res.,* **48,** 1423–1441.

——, P. Schlosser, and M. Visbeck, 2002: Rates and mechanisms of water mass transformation in the Labrador Sea as inferred from tracer observations. *J. Phys. Oceanogr.,* **32,** 666–686.

Klatt, O., and Coauthors, 2002: Repeated CFC sections at the Greenwich meridian in the Weddell Sea. *J. Geophys. Res.,* **107,** 3030, doi:10.1029/2000JC000731.

Ledwell, J. R., A. J. Watson, and C. S. Law, 1998: Mixing of a tracer in the pycnocline. *J. Geophys. Res.,* **103,** 21 499–21 530.

Maiss, M., and C. A. M. Brenninkmeijer, 1998: Atmospheric SF_6: Trends, sources, and prospects. *Environ. Sci. Technol.,* **32,** 3077–3086.

Molinari, R. L., R. A. Fine, W. D. Wilson, R. G. Curry, J. Abell, and M. S. McCartney, 1998: The arrival of recently formed Labrador Sea Water in the deep western boundary current at 26.5°N. *Geophys. Res. Lett.,* **25,** 2249–2252.

Neu, J. L., and R. A. Plumb, 1999: The age of air in "leaky pipe" model of stratospheric transport. *J. Geophys. Res.,* **104,** 19 243–19 255.

Pickart, R. S., and W. M. Smethie, 1998: Temporal evolution of the deep western boundary current where it enters the subtropical domain. *Deep-Sea Res.,* **45A,** 1053–1083.

——, N. G. Hogg, and W. M. Smethie, 1989: Determining the strength of the deep western boundary current using the chlorofluoromethane ratio. *J. Phys. Oceanogr.,* **19,** 940–951.

Prather, M. J., 1986: Numerical advectyion by conservation of second-order moments. *J. Geophys. Res.,* **91,** 6671–6681.

Rhein, M., 1994: The deep western boundary current—Tracers and velocities. *Deep-Sea Res.,* **41A,** 263–281.

Smethie, W. M., and R. A. Fine, 2001: Rates of North Atlantic Deep Water formation calculated from chlorofluorocarbon inventories. *Deep-Sea Res.,* **48A,** 189–215.

——, ——, A. Putzka, and E. P. Jones, 2000: Tracing the flow of North Atlantic Deep Water using chlorofluorocarbons. *J. Geophys. Res.,* **105,** 14 297–14 323.

Sonnerup, R. E., 2001: On the relations among CFC derived water mass ages. *Geophys. Res. Lett.,* **28,** 1739–1742.

Steinfeldt, R., and M. Rhein, 2004: Spreading velocities and dilution of North Atlantic Deep Water in the tropical Atlantic based on CFC time series. *J. Geophys. Res.,* **109,** C03046, doi:10.1029/2003JC002050.

Stramma, L., D. Kieke, M. Rhein, F. Schott, I. Yashayaev, and K. P. Koltermann, 2004: Deep water changes at the western boundary of the subpolar North Atlantic during 1996 to 2001. *Deep-Sea Res.,* **51,** 1033–1056.

Walker, S. J., R. F. Weiss, and P. K. Salameh, 2000: Reconstructed histories of the annual mean atmospheric mole fractions for the halocarbons CFC-11, CFC-12, CFC-113, and carbon tetrachloride. *J. Geophys. Res.,* **105,** 14 285–14 296.

Watts, D. R., 1991: Equatorward currents in temperatures 1.8–6.0C on the continental slope in the Mid-Atlantic Bight. *Deep Convection and Deep Water Formation in the Ocean,* P. C. Chu and J. C. Gascard, Eds., Elsevier Science, 183–196.

Waugh, D. W., T. M. Hall, and T. W. N. Haine, 2003: Relationships among tracer ages. *J. Geophys. Res.,* **108,** 3138, doi:10.1029/2002JC001325.

Wunsch, C., 2002: Oceanic age and transient tracers: Analytical and numerical solutions. *J. Geophys. Res.,* **107,** 3048, doi:10.1029/2001JC000797.

Yang, J., and T. M. Joyce, 2003: How do high-latitude North Atlantic climate signals the crossover between the deep western boundary current and the Gulf Stream? *Geophys. Res. Lett.,* **30,** 1070, doi:10.1029/2002GL015366.

Unauthenticated | Downloaded 05/20/24 05:05 AM UTC